

## Experimental Detection of the Correlation Rényi Entropy in the Central Spin Model

Mohamad Niknam<sup>1,2,3,\*</sup>, Lea F. Santos<sup>4</sup>, and David G. Cory<sup>1,5</sup>

<sup>1</sup>*Institute for Quantum Computing, University of Waterloo, Waterloo, Ontario, Canada N2L3G1*

<sup>2</sup>*Department of Physics, University of Waterloo, Waterloo, Ontario, Canada N2L3G1*

<sup>3</sup>*Department of Chemistry and Biochemistry, University of California Los Angeles, Los Angeles, California 90095-1059, USA*

<sup>4</sup>*Department of Physics, Yeshiva University, New York City, New York, 10016, USA*

<sup>5</sup>*Department of Chemistry, University of Waterloo, Waterloo, Ontario, Canada N2L3G1*



(Received 26 November 2020; revised 15 March 2021; accepted 15 July 2021; published 18 August 2021)

We propose and experimentally measure an entropy that quantifies the volume of correlations among qubits. The experiment is carried out on a nearly isolated quantum system composed of a central spin coupled and initially uncorrelated with 15 other spins. Because of the spin-spin interactions, information flows from the central spin to the surrounding ones forming clusters of multispin correlations that grow in time. We design a nuclear magnetic resonance experiment that directly measures the amplitudes of the multispin correlations and use them to compute the evolution of what we call correlation Rényi entropy. This entropy keeps growing even after the equilibration of the entanglement entropy. We also analyze how the saturation point and the timescale for the equilibration of the correlation Rényi entropy depend on the system size.

DOI: [10.1103/PhysRevLett.127.080401](https://doi.org/10.1103/PhysRevLett.127.080401)

Which microscopic entropy can capture the changes undergone by an isolated quantum system that evolves in time? The von Neumann entropy for the entire density matrix of the system is not an appropriate choice, because it is constant in isolated systems. A common approach is to trace out part of the system and resort to the entanglement entropy, which quantifies the degree of entanglement between the traced-out part and the remaining subsystem. Despite the challenges presented by this quantity, it has been experimentally measured in a system with three superconducting qubits after tomographically reconstructing the evolved density matrix [1], in a Bose-Hubbard system with six cold atoms and site-resolved number statistics [2], and in a chain with 20 trapped ions where the entropy of subsystems with up to ten ions is obtained through randomized measurements [3]. The entanglement entropy is bounded by the quantum Fisher information, and this quantity also offers a way to detect the flow of information [4,5]. It has been experimentally measured with trapped ions [6] and in nuclear magnetic resonance (NMR) [7].

Another entropy that has received more theoretical than experimental attention is the participation Rényi entropy, which measures the spread in time of a nonstationary state in the Hilbert space. The system is usually prepared in a certain basis vector, and the entropy is computed by summing the squares of the probabilities for finding the system in its initial quantum state and in each one of the other basis vectors [8]. Common questions that are addressed with both the participation Rényi entropy and the entanglement entropy include the conditions for linear

or logarithmic growth in association with quantum chaos [9–13] or the transition to many-body localization [14–18], comparisons between their saturation values and thermodynamic entropies in studies of thermalization [2,19], and analytic predictions for the spread of entanglement [20–23]. One of the differences between the two entropies is that the participation Rényi entropy is extensive in the Hilbert space size of the composite system, while the maximum value of the entanglement entropy does not change if the size of the subsystem remains fixed.

In this Letter, we propose a third alternative that we measure employing NMR coherence detection techniques. NMR has been used to investigate questions in many-body quantum dynamics, such as many-body localization [24], prethermalization [25,26], and the scrambling of quantum information [7,27,28]. Our experiment demonstrates that NMR platforms are also test beds for the analysis of entropy growth.

Our entropy quantifies the growth of the volume of correlations as information flows from a central spin (qubit) to its surrounding spins. As devices with ever larger numbers of qubits become operational, a detailed picture of how quantum information flows and how the dynamics saturates is essential for designing and controlling quantum processors. This understanding is also necessary for classical simulations, which become impracticable under a substantial growth of correlations.

In our sample, the central spin is initially polarized and coupled with 15 unpolarized surrounding spins. This composite system is at room temperature and nearly isolated from external environments. The experiment

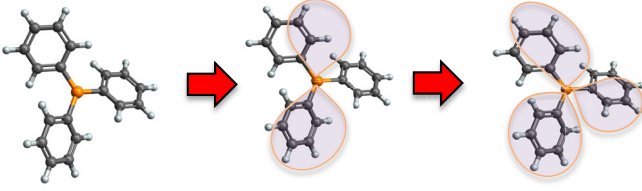


FIG. 1. Schematic illustration of the flow of information initially contained in the central spin (orange circle) to the surrounding 15 spins. Each shaded area indicates a cluster of correlated spins.

employs two main ingredients available to solid-state NMR. One is the possibility to coherently average out the interactions among the surrounding spins, so that the remaining effective Hamiltonian contains only the interactions of those spins with the central one. Because of these couplings, as we sketch in Fig. 1, information that is initially concentrated in the central spin (orange circle) flows to the surrounding spins and gives rise to clusters of multispin correlations (shades) that grow in time. The second important element of the experiment is the possibility to collectively rotate the spins and perform a basis transformation that allows us to monitor the growth of multispin correlations by probing only the central spin [7,29,30].

Multispin correlations were used in Ref. [24] to measure the average correlation length and estimate the entanglement entropy in spin chains. Here, we use the amplitudes of the multispin correlations to compute what we call correlation Rényi entropy. We find that after the saturation of the entanglement entropy, the correlation Rényi entropy keeps growing for times 1 order of magnitude longer, during which the larger clusters of multispin correlations build up. The experimental results show excellent agreement with our numerical simulations. We also perform a scaling analysis of the growth rate, the saturation value, and the equilibration time of the correlation Rényi entropy. Both the rate and the saturation point grow logarithmically as the size of the composite system increases, while the equilibration time is nearly independent of system size.

*Experimental System.*—We work with a polycrystalline solid made of an ensemble of triphenylphosphine molecules. Each molecule has a central  $^{31}\text{P}$  nuclear spin coupled to  $^1\text{H}$  spins via the heteronuclear dipolar interaction

$$H_{\text{CSB}} = \sum_j^N \omega_j \sigma_z^{\text{CS}} \otimes \sigma_z^j \otimes \mathbb{1}^{\otimes N-1}, \quad (1)$$

where CSB stands for the composite system made of the central spin (CS) and a finite bath ( $B$ ) with  $N = 15$  surrounding spins, and  $\sigma_z^j$  is the Pauli matrix for the  $j$ th bath spin. The coupling constants  $\omega_j$  are determined by the orientation and the distance of the bath spins from the central spin, the majority having values below 1200 Hz (see distribution in [7]).

The initial density matrix of the composite system is  $\rho(0) = \rho^{\text{CS}}(0) \otimes \rho^B(0)$ . Quantum information resides initially in the central spin, which is in the state  $\rho^{\text{CS}}(0) = (1 + \epsilon \sigma_x)/2$ , where  $\epsilon \sim 10^{-5}$  is the nuclear spin polarization at room temperature, while the surrounding spins are in a fully mixed state  $\rho^B(0) = (1/2)^{\otimes N}$ . The homonuclear dipolar interactions among the bath spins are averaged out by applying the MREV-8 pulse sequence, which is named after Mansfield, Rhim, Elleman and Vaughan [31–33]. During the entire time span of our experiment, the effects of external environments are also under control [7], so that the evolution of the density matrix of the composite system,  $\rho(T) = U_{\text{CSB}}(T)\rho(0)U_{\text{CSB}}^\dagger(T)$ , is effectively described by the unitary propagator  $U_{\text{CSB}}(T) = e^{-iH_{\text{CSB}}T}$ . As the CSB system evolves under the ZZ interaction, information from the central spin gets shared with the bath spins giving rise to clusters of multispin correlations.

*FID and Entanglement Entropy.*—The loss of information from the central spin can be quantified with the free induction decay (FID). For a single molecule, it is given by

$$\text{FID}(T) = \text{Tr}\{\sigma_x^{\text{CS}} \rho^{\text{CS}}(T)\} = \frac{\epsilon}{2^{N+1}} \sum_{k=1}^{2^{N+1}} \cos(2\langle \varphi_k | H_{\text{CSB}} | \varphi_k \rangle T), \quad (2)$$

where  $\rho^{\text{CS}}(T) = \text{Tr}_B[\rho(T)]$  and  $|\varphi_k\rangle$  is one of the  $2^{N+1}$  spin configurations in the  $z$  direction, such as  $|\uparrow\downarrow\downarrow\dots\uparrow\rangle$ .

The total NMR signal is induced by an ensemble of molecules with typically more than  $10^{17}$  spins. The normalized total signal is obtained by setting  $\epsilon$  to 1 and is therefore what we would obtain also with a fully polarized central spin, where  $\rho^{\text{CS}}(0) = (1 + \sigma_x)/2$ .

The results from numerical simulations for  $N = 15$  are shown in Fig. 2(a). Thin lines correspond to representative random orientations of the molecules, and the thick curve gives the average of 300 random realizations of the principle axis orientation of the molecule [34]. The curve for the ensemble average is smooth and quickly saturates at  $\bar{F} \sim 0$ .

The entanglement entropy between the central spin and the bath is a function of the FID,

$$S_{\text{ent}}(T) = -\text{Tr}\{\rho^{\text{CS}}(T) \log_2[\rho^{\text{CS}}(T)]\} = -[f^+(T) \log_2 f^+(T) + f^-(T) \log_2 f^-(T)], \quad (3)$$

where  $f^\pm(T) = (1/2) \pm \text{FID}(T)/2$ . For the weakly polarized central spin of our experiment, the entanglement entropy shows a minor change from  $S_{\text{ent}}(0) \sim 1 - \epsilon^2/2$  to  $S_{\text{ent}}(T \gg 0) \sim 1$ . However, to provide a more general comparison between  $S_{\text{ent}}(T)$ ,  $\text{FID}(T)$ , and our entropy, we show in Fig. 2(b) the entanglement entropy obtained with a fully polarized central spin. Similarly to the FID,  $S_{\text{ent}}(T)$  evolves quickly and then saturates at the maximum entropy value  $\bar{S}_{\text{ent}} \sim 1$ . For both quantities, the saturation of the

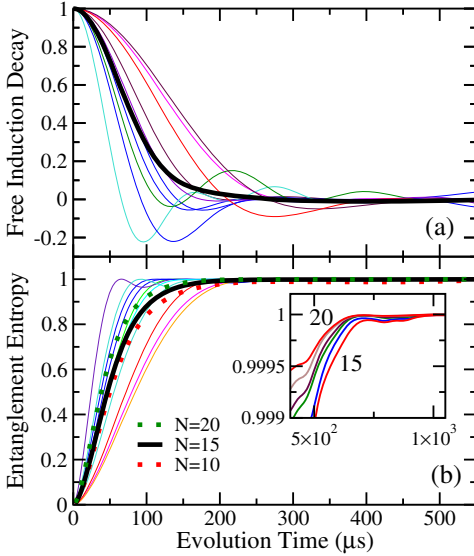


FIG. 2. Free induction decay (a) and entanglement entropy (b) for a central spin coupled with 15 surrounding spins via the ZZ interaction in Eq. (1). Thin lines are for each realization of  $\omega_j$ , and a thick line gives the average of over 300 random orientations of the molecules. The dotted lines in (b) also give the ensemble average for  $N = 10$  and  $N = 20$ . Inset of panel (b): averaged entangled entropy for  $N = 15, 16, \dots, 20$  from bottom to top.

dynamics happens at  $T \sim 200 \mu\text{s}$ . In Fig. 2(b), we also show with dotted lines ensemble averages for  $N = 10$  and  $N = 20$ . The slope of  $S_{\text{ent}}(T)$  increases with system size, which suggests that the saturation should happen earlier for larger spin baths. In what follows, we compare these timescales with the saturation time obtained for the correlation Rényi entropy.

**Multispin Correlations.**—The evolution of the total density matrix is given by

$$\begin{aligned} \rho(T) &= e^{-iH_{\text{CSB}}T} \rho(0) e^{iH_{\text{CSB}}T} \\ &= \rho(0) + iT[\rho(0), H_{\text{CSB}}] \\ &\quad - \frac{T^2}{2} \{[\rho(0), H_{\text{CSB}}], H_{\text{CSB}}\} + \dots \end{aligned} \quad (4)$$

The commutators above lead to terms with a different number  $m$  of nonidentity bath spins operators. By arranging these terms together,  $\rho(T)$  for a single molecule is

$$\begin{aligned} \rho(T) &= \frac{1}{2^{N+1}} \left\{ \mathbb{1}^{\otimes N+1} + \epsilon C_0^z(T) \sigma_x^{\text{CS}} \otimes \mathbb{1}^{\otimes N} \right. \\ &\quad + \epsilon \sum_j C_1^{z(j)}(T) \sigma_y^{\text{CS}} \otimes \sigma_z^j \otimes \mathbb{1}^{\otimes N-1} \\ &\quad \left. + \epsilon \sum_{j_1 < j_2} C_2^{z(j_1 j_2)}(T) \sigma_x^{\text{CS}} \otimes \sigma_z^{j_1} \otimes \sigma_z^{j_2} \otimes \mathbb{1}^{\otimes N-2} + \dots \right\}, \end{aligned} \quad (5)$$

where  $C_m^{z(j_1 j_2 \dots j_m)}$  is the amplitude of the clusters with the same  $m$  (see a detailed example for  $N = 2$  in Supplemental Material [34]). At  $T = 0$ ,  $C_0^z(0) = 1$  and  $C_{m \neq 0}^{z(j_1 j_2 \dots j_m)}(0) = 0$ . For  $T > 0$ , the amplitudes for the terms with  $m > 0$  increase, indicating that clusters of correlated spins build up and grow.

The uncorrelated term with amplitude  $C_0^z(T)$  is the only one that survives the partial trace used to obtain  $\rho^{\text{CS}}(T)$  in Eq. (2) and therefore the only one that contributes to  $\text{FID}(T)$ . This is also the case for the entanglement entropy, since both quantities are related [Eq. (3)]. The decay of  $C_0^z(T)$  describes the loss of information from the central spin, which causes the decline of the observable NMR signal and the growth of the entanglement entropy. *However, to better understand the dynamics of the composite system, one needs a quantity that also captures the buildup of multispin correlations as determined by the higher order terms with  $m > 0$ .*

The NMR experiment is designed to measure the coherence order intensities. To explain what this means and how the measurement is done, let us write the bath spin operators in Eq. (5) in terms of coherence raising and lowering operators in the x-quantization basis  $\sigma_{\pm}^x := (\sigma_y \pm i\sigma_z)/\sqrt{2}$  [35]. The term  $\sigma_x^{\text{CS}} \sigma_z^{j_1} \sigma_z^{j_2}$ , for example, expands into four terms,  $-1/2 \{ \sigma_x^{\text{CS}} \sigma_+^{xj_1} \sigma_+^{xj_2} + \sigma_x^{\text{CS}} \sigma_-^{xj_1} \sigma_-^{xj_2} - \sigma_x^{\text{CS}} \sigma_+^{xj_1} \sigma_-^{xj_2} - \sigma_x^{\text{CS}} \sigma_-^{xj_1} \sigma_+^{xj_2} \}$ . The difference between the number  $n_+$  of  $\sigma_+^x$  operators and the number  $n_-$  of  $\sigma_-^x$  operators defines the coherence order  $n = n_+ - n_-$ . Therefore, the first one of those four terms above has coherence order  $n = 2$ , the second one has  $n = -2$ , and the last two have  $n = 0$ .

According to the coherence orders, Eq. (5) becomes

$$\begin{aligned} \rho(T) &= \frac{1}{2^{N+1}} \left\{ \mathbb{1}^{\otimes N+1} + \epsilon \sum_k C_0^{x,k}(T) \rho_0^{x,k} \right. \\ &\quad + \epsilon \sum_k [C_{+1}^{x,k}(T) \rho_{+1}^{x,k} + C_{-1}^{x,k}(T) \rho_{-1}^{x,k}] \\ &\quad \left. + \epsilon \sum_k [C_{+2}^{x,k}(T) \rho_{+2}^{x,k} + C_{-2}^{x,k}(T) \rho_{-2}^{x,k}] + \dots \right\}, \end{aligned} \quad (6)$$

where  $\rho_n^{x,k}$  represents each term with coherence order  $n$  (see Supplemental Material [34]). Our experiment directly measures the intensities  $|C_n^x(T)|^2 = \sum_k |C_n^{x,k}(T)|^2$ .

The essence of the coherence detection technique is to exploit the collective response of the spins. At time  $T$ , we apply the encoding pulse  $R_x(\phi) = \exp(i(\phi/2) \sum_j \mathbb{1}^{\text{CS}} \otimes \mathbb{1}^1 \otimes \dots \otimes \sigma_x^j \otimes \dots \otimes \mathbb{1}^N)$  that collectively rotates the bath spins by an angle  $\phi$  [29,30,36]. The purpose of this operation is to encode each coherence order in a phase factor  $e^{in\phi}$  (see Supplemental Material [34]). Subsequently, the CSB dynamics is reversed by applying a  $\pi$  pulse to the central spin, and the composite system is evolved for another interval  $T$ . After the echo, the resulting density matrix at  $2T$  is [34]

$$\rho_\phi(2T) = \frac{1}{2^{N+1}} \left\{ \mathbb{1}^{\otimes N+1} + \epsilon \sum_{n=-N}^N e^{in\phi} |C_n^x(T)|^2 \sigma_x^{\text{CS}} \otimes \mathbb{1}^{\otimes N} \right\}, \quad (7)$$

and the observed NMR signal for a single molecule is  $S(2T) = \text{Tr}[\text{Tr}_B[\rho_\phi(2T)]\sigma_x^{\text{CS}}]$ . Just as in the case of  $\text{FID}(T)$ , the total signal is obtained for a large ensemble of molecules.

The signal is recorded for various increments of rotation angle  $\phi \in [0, 2\pi]$ . By performing a Fourier transform of this array of observed signals, we obtain the intensities  $|C_n^x(T)|^2$ , with  $\sum_{n=-N}^N |C_n^x(T)|^2 = 1$ . Note that the NMR experiment is designed so that all the information about the coherence orders is contained in the central spin, which is the only spin experimentally probed.

The evolution of the coherence orders' intensities is shown in Fig. 3(a). The agreement between the experimental data and the numerical simulations for orders up to  $n = -6$ , 6 is excellent. Higher order terms develop at even longer times and are more challenging to detect experimentally. This figure reveals the details of how information lost from the central spin gets shared with the surrounding qubits.

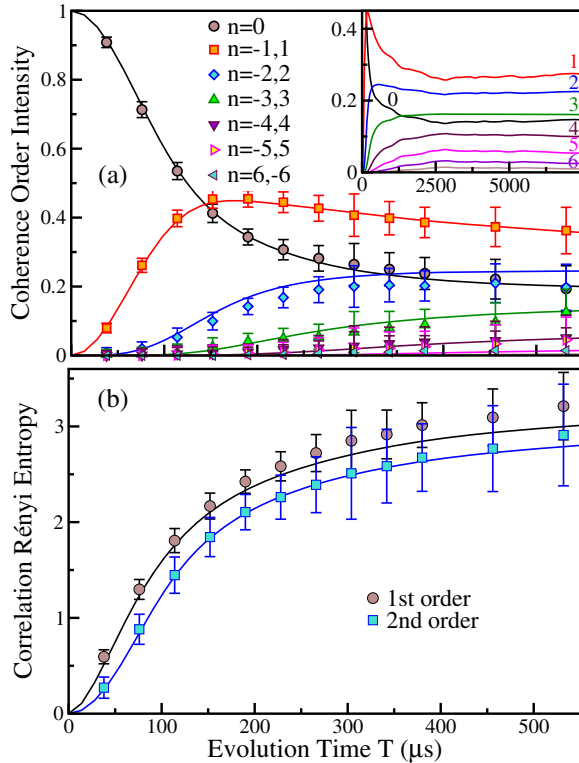


FIG. 3. Evolution of the coherence orders' intensities  $|C_n^x(T)|^2$  in (a) and for a longer time in the inset, and the first and second order correlation Rényi entropies in (b). Symbols represent the experimental data, and solid lines give the numerical results for  $N = 15$  averaged over 300 orientations of the molecule.

*Correlation Rényi Entropies.*—We use the coherence order intensities  $|C_n^x(T)|^2$  to compute the correlation Rényi entropy. The first and second order correlation Rényi entropies are respectively defined as

$$S_1 = - \sum_{n=-N}^N |C_n^x(T)|^2 \log_2 |C_n^x(T)|^2, \quad (8)$$

$$S_2 = - \log_2 \left( \sum_{n=-N}^N |C_n^x(T)|^4 \right). \quad (9)$$

They describe the growth of multispin coherences. The absence of correlations implies that  $S_1^{\min} = S_2^{\min} = 0$ , while the homogeneous distribution of coherence orders, that is,  $|C_n^x(T)|^2 = (2N+1)^{-1}$ , leads to the maximum value,  $S_1^{\max} = S_2^{\max} = \log_2(2N+1)$ .

The experimental data for both entropies are compared with numerical simulations in Fig. 3(b). One sees that the growth of  $S_{1,2}$  is not complete during the timescale of our experiment. The correlation Rényi entropy keeps increasing for  $T > 500 \mu\text{s}$ , implying that the growth of the volume of correlations has not yet ceased and correlations of higher orders are still developing. In fact, as the simulations for different bath sizes in the inset of Fig. 4(a) indicate, saturation happens at  $T \sim 2000 \mu\text{s}$ . This contrasts with the entanglement entropy displayed in Fig. 2(b), where the curves are already flat for times 1 order of magnitude shorter, at  $T \sim 200 \mu\text{s}$ .

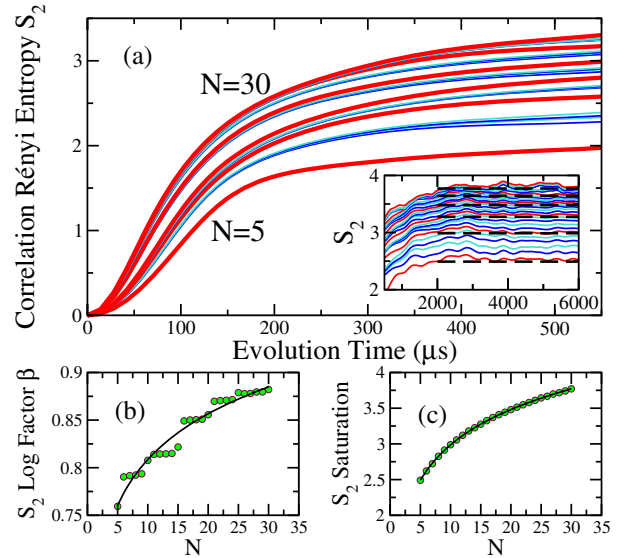


FIG. 4. (a) Evolution of the correlation Rényi entropy  $S_2$  for  $N = 5, \dots, 30$  averaged over various orientations of the molecules. The thick red lines correspond to bath sizes that are multiples of 5. Inset in (a): solid lines correspond to the curves of  $S_2(T)$  up to saturation and the dashed lines indicate  $\bar{S}_2$ . (b) Scaling analysis of the factor  $\beta$  in  $S_2(T) \sim -4.18 + \beta \log_2(T)$  (symbols) fitted with  $0.65 + 0.07 \ln(N)$  (solid line). (c) Scaling analysis of the saturation values of  $S_2$  (symbols) fitted with  $1.34 + 0.71 \ln(N)$  (solid line).

The discrepancy between the timescales for the equilibration of  $S_{1,2}$  and  $S_{\text{ent}}$  motivated us to have a closer look at the saturation of the entanglement entropy. By significantly increasing the scale in the  $y$  axis of Fig. 2(b), we observe in the inset that  $S_{\text{ent}}$  for different bath sizes actually keeps increasing for  $T > 200 \mu\text{s}$ . It is only because we have a detailed picture of the growth of the volume of correlations, that we could have expected the existence of this residual increase. The evolution of the entanglement entropy, just as the FID, reflects the loss of information from the central spin, as characterized by the decay of  $C_0^z(T)$ , and this decay happens simultaneously with the growth of the higher order correlations. While the necessary precision to detect the growth of  $S_{\text{ent}}$  for  $T > 200 \mu\text{s}$  would be experimentally unreachable, the experimental increase of the Rényi entropies  $S_{1,2}$  at these timescales is evident in Fig. 3(b).

*Equilibration.*—The complete saturation of the correlation Rényi entropy takes place once the clusters of correlated spins stop growing, that is, when the coherence orders' intensities become constant, as seen in the inset of Fig. 3(a). To estimate the timescale for the equilibration and how it depends on the bath size, we study numerically in Fig. 4(a) the evolution of  $S_2$  for baths ranging from  $N = 5$  to  $N = 30$ .

We compute the saturation value of the entropy,  $\bar{S}_2$ , by averaging the values of  $S_2(T)$  for  $T > 5000 \mu\text{s}$ , when the curves are clearly flat, as seen in the inset of Fig. 4(a). We then obtain the equilibration times  $T_{\text{eq}}$  by verifying where each numerical curve of  $S_2(T)$  first crosses its saturation point. We find that  $T_{\text{eq}} = (2052.1 \pm 163.7) \mu\text{s}$  for  $N = 5, \dots, 30$ .

The fact that  $T_{\text{eq}}$  is nearly independent of the system size happens because both the growth rate of  $S_2(T)$  and its saturation value scale as  $\ln(N)$ . This is verified by fitting the evolution of  $S_2$  in the interval  $50 \mu\text{s} < T < 300 \mu\text{s}$  with the logarithmic function  $\alpha + \beta \log_2(x)$ , where  $\alpha$  and  $\beta$  are fitting constants. The fitting improves for larger system sizes, and we find that the factor  $\beta$  increases as  $\ln(N)$ , as shown in Fig. 4(b). And the scaling analysis in Fig. 4(c) confirms that  $\bar{S}_2$  also increases as  $\ln(N)$ .

*Conclusion.*—We introduced and experimentally measured the correlation Rényi entropy. This is a novel entropy measure that relies on the volume of multispin correlations. While the entanglement entropy  $S_{\text{ent}}$  quantifies the loss of information from the central spin, the correlation Rényi entropy  $S_{1,2}$  provides a more detailed picture of the dynamics of the composite system by capturing how that information gets shared between the central spin and the bath spins through the correlations. Most notably,  $S_{1,2}$  saturates at a time that is 1 order of magnitude larger than the saturation time for  $S_{\text{ent}}$ .

The correlation Rényi entropy opens interesting perspectives for the experimental detection of many-body correlations growth and the spread of quantum information in quantum devices. The experimental resources needed to

measure this entropy scales linearly with the size of the composite system, and the only requirements are that the evolution Hamiltonian can be inverted and that the spins can be collectively rotated. We also expect applications in quantum error correction codes, where information is encoded in long-range quantum many-body states, and in the detection of the propagation speed of correlations.

M. N. and L. F. S. thank the Simons Center for Geometry and Physics at Stony Brook University, where some of the research for this Letter was performed. L. F. S. is supported by the NSF Grant No. DMR-1936006. The research results communicated here would not be possible without the significant contributions of the Canada First Research Excellence Fund.

\*Corresponding author.  
mniknam@gmail.com

- [1] C. Neill *et al.*, Ergodic dynamics and thermalization in an isolated quantum system, *Nat. Phys.* **12**, 1037 (2016).
- [2] A. M. Kaufman, M. Eric Tai, A. Lukin, M. Rispoli, R. Schittko, P. M. Preiss, and M. Greiner, Quantum thermalization through entanglement in an isolated many-body system, *Science* **353**, 794 (2016).
- [3] T. Brydges, A. Elben, P. Jurcevic, B. Vermersch, C. Maier, B. P. Lanyon, P. Zoller, R. Blatt, and C. F. Roos, Probing Rényi entanglement entropy via randomized measurements, *Science* **364**, 260 (2019).
- [4] X.-M. Lu, X. Wang, and C. P. Sun, Quantum fisher information flow and non-markovian processes of open systems, *Phys. Rev. A* **82**, 042103 (2010).
- [5] M. Gärtner, P. Hauke, and A. Maria Rey, Relating Out-of-Time-Order Correlations to Entanglement via Multiple-Quantum Coherences, *Phys. Rev. Lett.* **120**, 040402 (2018).
- [6] J. Smith, A. Lee, P. Richerme, B. Neyenhuis, P. W. Hess, P. Hauke, M. Heyl, D. A. Huse, and C. Monroe, Many-body localization in a quantum simulator with programmable random disorder, *Nat. Phys.* **12**, 907 (2016).
- [7] M. Niknam, L. F. Santos, and D. G. Cory, Sensitivity of quantum information to environment perturbations measured with a nonlocal out-of-time-order correlation function, *Phys. Rev. Research* **2**, 013200 (2020).
- [8] V. V. Flambaum and F. M. Izrailev, Entropy production and wave packet dynamics in the fock space of closed chaotic many-body systems, *Phys. Rev. E* **64**, 036220 (2001).
- [9] C. T. Asplund and A. Bernamonti, Mutual information after a local quench in conformal field theory, *Phys. Rev. D* **89**, 066015 (2014).
- [10] E. Bianchi, L. Hackl, and N. Yokomizo, Linear growth of the entanglement entropy and the kolmogorov-sinai rate, *J. High Energy Phys.* **03** (2018) 25.
- [11] L. F. Santos, F. Borgonovi, and F. M. Izrailev, Chaos and Statistical Relaxation in Quantum Systems of Interacting Particles, *Phys. Rev. Lett.* **108**, 094102 (2012).
- [12] L. Vidmar and M. Rigol, Entanglement Entropy of Eigenstates of Quantum Chaotic Hamiltonians, *Phys. Rev. Lett.* **119**, 220603 (2017).

- [13] F. Borgonovi, F. M. Izrailev, and L. F. Santos, Exponentially fast dynamics of chaotic many-body systems, *Phys. Rev. E* **99**, 010101(R) (2019).
- [14] M. Žnidarič, T. Prosen, and P. Prelovšek, Many-body localization in the Heisenberg XXZ magnet in a random field, *Phys. Rev. B* **77**, 064426 (2008).
- [15] J. H. Bardarson, F. Pollmann, and J. E. Moore, Unbounded Growth of Entanglement in Models of Many-Body Localization, *Phys. Rev. Lett.* **109**, 017202 (2012).
- [16] E. J. Torres-Herrera and L. F. Santos, Extended nonergodic states in disordered many-body quantum systems, *Ann. Phys. (Amsterdam)* **529**, 1600284 (2017).
- [17] A. Lukin, M. Rispoli, R. Schittko, M. Eric Tai, A. M. Kaufman, S. Choi, V. Khemani, J. Léonard, and M. Greiner, Probing entanglement in a many-body-localized system, *Science* **364**, 256 (2019).
- [18] M. Daumann, R. Steinigeweg, and T. Dahm, Many-body localization in translational invariant diamond ladders with flat bands, [arXiv:2009.09705](https://arxiv.org/abs/2009.09705).
- [19] L. F. Santos, A. Polkovnikov, and M. Rigol, Weak and strong typicality in quantum systems, *Phys. Rev. E* **86**, 010102(R) (2012).
- [20] D. N. Page, Average Entropy of a Subsystem, *Phys. Rev. Lett.* **71**, 1291 (1993).
- [21] L. Vidmar, L. Hackl, E. Bianchi, and M. Rigol, Entanglement Entropy of Eigenstates of Quadratic Fermionic Hamiltonians, *Phys. Rev. Lett.* **119**, 020601 (2017).
- [22] V. Alba and P. Calabrese, Entanglement and thermodynamics after a quantum quench in integrable systems, *Proc. Natl. Acad. Sci. U.S.A.* **114**, 7947 (2017).
- [23] P. Calabrese, Entanglement spreading in non-equilibrium integrable systems, *SciPost Phys. Lect. Notes* **20** (2020).
- [24] K. Xuan Wei, C. Ramanathan, and P. Cappellaro, Exploring Localization in Nuclear Spin Chains, *Phys. Rev. Lett.* **120**, 070501 (2018).
- [25] K. Xuan Wei, P. Peng, O. Shtanko, I. Marvian, S. Lloyd, C. Ramanathan, and P. Cappellaro, Emergent Prethermalization Signatures in Out-of-Time Ordered Correlations, *Phys. Rev. Lett.* **123**, 090605 (2019).
- [26] C. Yin, P. Peng, X. Huang, C. Ramanathan, and P. Cappellaro, Prethermal quasiconserved observables in floquet quantum systems, *Phys. Rev. B* **103**, 054305 (2021).
- [27] J. Li, R. Fan, H. Wang, B. Ye, B. Zeng, H. Zhai, X. Peng, and J. Du, Measuring Out-of-Time-Order Correlators on a Nuclear Magnetic Resonance Quantum Simulator, *Phys. Rev. X* **7**, 031011 (2017).
- [28] C. M. Sánchez, A. K. Chattah, K. X. Wei, L. Buljubasich, P. Cappellaro, and H. M. Pastawski, Perturbation Independent Decay of the Loschmidt Echo in a Many-Body System, *Phys. Rev. Lett.* **124**, 030601 (2020).
- [29] C. Ramanathan, H. Cho, P. Cappellaro, G. S. Boutis, and D. G. Cory, Encoding multiple quantum coherences in non-commuting bases, *Chem. Phys. Lett.* **369**, 311 (2003).
- [30] H. Cho, T. D. Ladd, J. Baugh, D. G. Cory, and C. Ramanathan, Multispin dynamics of the solid-state NMR free induction decay, *Phys. Rev. B* **72**, 054427 (2005).
- [31] U. Haeberlen, *High Resolution NMR in Solids: Selective Averaging* (Academic Press, New York, 1976).
- [32] W-K. Rhim, D. D. Elleman, and R. W. Vaughan, Enhanced resolution for solid state NMR, *J. Chem. Phys.* **58**, 1772 (1973).
- [33] B. C. Gerstein and C. R. Dybowski, *Transient Techniques in NMR of Solids* (Academic Press, Inc., New York, 1985).
- [34] See Supplemental Material at <http://link.aps.org/supplemental/10.1103/PhysRevLett.127.080401> for details of the experiment and a description of the coherence order detection technique.
- [35] S. S. Somaroo, D. G. Cory, and T. F. Havel, Expressing the operations of quantum computing in multiparticle geometric algebra, *Phys. Lett. A* **240**, 1 (1998).
- [36] J. Baum, M. Munowitz, A. N. Garroway, and A. Pines, Multiple-quantum dynamics in solid state NMR, *J. Chem. Phys.* **83**, 2015 (1985).